

Scalable preparation of water-soluble ink of few-layered WSe_2 nanosheets for large-area electronics

Guoyu Xian(冼国裕), Jianshuo Zhang(张建烁), Li Liu(刘丽), Jun Zhou(周俊), Hongtao Liu(刘洪涛), Lihong Bao(鲍丽宏), Chengmin Shen(申承民), Yongfeng Li(李永峰), Zhihui Qin(秦志辉), Haitao Yang(杨海涛)

Citation: Chin. Phys. B . 2020, 29(6): 066802 . **doi:** 10.1088/1674-1056/ab889e
Journal homepage: http://cpb.iphy.ac.cn; http://iopscience.iop.org/cpb

What follows is a list of articles you may be interested in

Adsorption behavior of triphenylene on Ru(0001) investigated by scanning tunneling microscopy

Li-Wei Jing(井立威), Jun-Jie Song(宋俊杰), Yu-Xi Zhang(张羽溪), Qiao-Yue Chen(陈乔悦), Kai-Kai Huang(黄凯凯), Han-Jie Zhang(张寒洁), Pi-Mo He(何丕模)

Chin. Phys. B . 2019, 28(7): 076801 . **doi:** 10.1088/1674-1056/28/7/076801

Interface effect on structural and electronic properties of graphdiyne adsorbed on SiO_2 and h-BN substrates: A first-principles study

Dong Bao-Juan, Yang Teng, Wang Ji-Zhang, Zhang Zhi-Dong

Chin. Phys. B . 2015, 24(9): 096806 . **doi:** 10.1088/1674-1056/24/9/096806

Performance improvement in polymeric thin film transistors using chemically modified both silver bottom contacts and dielectric surfaces

Xie Ying-Tao, Ouyang Shi-Hong, Wang Dong-Ping, Zhu Da-Long, Xu Xin, Tan Te, Fong Hon-Hang

Chin. Phys. B . 2015, 24(9): 096803 . **doi:** 10.1088/1674-1056/24/9/096803

Scanning tunneling microscopy study of molecular growth structures of $Gd@C_{82}$ on Cu(111)

Chen Jian, Qin Zhi-Hui, Pan Jin-Bo, Lu Shuang-Zan, Du Shi-Xuan, Gao Hong-Jun, Cao Geng-Yu

Chin. Phys. B . 2013, 22(7): 076802 . **doi:** 10.1088/1674-1056/22/7/076802

Kinetic Monte Carlo simulations of optimization of self-assembly quantum rings growth strategy based on substrate engineering

Liu Jian-Tao, Feng Hao, Yu Zhong-Yuan, Liu Yu-Min, Shi Qiang, Song Xin, Zhang Wen, Peng Yi-Wei

Chin. Phys. B . 2013, 22(4): 046801 . **doi:** 10.1088/1674-1056/22/4/046801

Scalable preparation of water-soluble ink of few-layered WSe_2 nanosheets for large-area electronics*

Guoyu Xian(冼国裕)[1,2], Jianshuo Zhang(张建烁)[2,3,†], Li Liu(刘丽)[1], Jun Zhou(周俊)[2], Hongtao Liu(刘洪涛)[2], Lihong Bao(鲍丽宏)[2], Chengmin Shen(申承民)[2], Yongfeng Li(李永峰)[3], Zhihui Qin(秦志辉)[1,§], and Haitao Yang(杨海涛)[2,†‡]

[1] *Key Laboratory for Micro/Nano Optoelectronic Devices of Ministry of Education & Hunan Provincial Key Laboratory of Low-Dimensional Structural Physics and Devices, School of Physics and Electronics, Hunan University, Changsha* 410082, *China*

[2] *Beijing National Laboratory for Condensed Matter Physics, Institute of Physics, Chinese Academy of Sciences, Beijing* 100190, *China*

[3] *State Key Laboratory of Heavy Oil Processing, China University of Petroleum, Beijing* 102249, *China*

(Received 27 March 2020; revised manuscript received 2 April 2020; accepted manuscript online 12 April 2020)

Few-layer two-dimensional (2D) semiconductor nanosheets with a layer-dependent band gap are attractive building blocks for large-area thin-film electronics. A general approach is developed to fast prepare uniform and phase-pure 2H-WSe_2 semiconducting nanosheets at a large scale, which involves the supercritical carbon dioxide (SC-CO_2) treatment and a mild sonication-assisted exfoliation process in aqueous solution. The as-prepared 2H-WSe_2 nanosheets preserve the intrinsic physical properties and intact crystal structures, as confirmed by Raman, x-ray photoelectron spectroscopy (XPS), and scanning transmission electron microscope (STEM). The uniform 2H-WSe_2 nanosheets can disperse well in water for over six months. Such good dispersivity and uniformity enable these nanosheets to self-assembly into thickness-controlled thin films for scalable fabrication of large-area arrays of thin-film electronics. The electronic transport and photoelectronic properties of the field-effect transistor based on the self-assembly 2H-WSe_2 thin film have also been explored.

Keywords: low dimensional, nanosheets, self-assembly, electronics

PACS: 68.65.−k, 62.23.Kn, 81.16.Dn, 77.55.df **DOI:** 10.1088/1674-1056/ab889e

1. Introduction

Ultra-thin two-dimensional (2D) transition metal dichalcogenides (TMDs), exhibiting unique electronic properties that are absent in bulk due to the geometrical confinement, distinct crystal symmetry, and natural out-of-plane self-terminating surfaces without dangling bonds, have demonstrated immense potential for diverse applications, including electronics, optoelectronics, and catalysis.[1–4] Depending on the selection of metal and chalcogen species, TMDs can be semiconducting (e.g., MoS_2, WSe_2), metallic (e.g., NbS_2, $TaSe_2$), or semimetallic (e.g., WTe_2). Combining with other 2D materials with diverse insulating (h-BN), metallic (graphene), and superconducting ($NbSe_2$) properties, TMDs nanosheets with layer-dependent band gaps would be very attractive building blocks for large-area printed and flexible thin-film devices.[5,6]

A wide variety of TMDs nanosheets can be produced by liquid-phase exfoliation. This technique brings considerable advantages: This method is robust, can be carried out in ambient conditions, is scalable, allows the preparation of films, hybrids, and composites, and may facilitate processing by using standard technologies such as reel-to-reel manufacturing to apply in large-area thin-film electronics.[7,8] Chemical intercalation, as a widely-used liquid-phase exfoliation method mostly using n-butyllithium (n-BuLi) as a lithiation agent, is a versatile method to prepare few-layer TMDs nanosheets. The troublesome issues with this method are that the lithium intercalation is time-consuming and extremely sensitive to the environmental conditions. Furthermore, the residual lithium ions induce structural deformations in some TMDs, typically the formation of 1T phase, resulting in poor electrical performance.[9,10] The ultrasonication assisted liquid exfoliation method developed by Coleman *et al.* can facilely prepare nanosheets from various TMDs bulk materials.[4] Specifically, the surface energies of TMDs are about 46–65 $mJ{\cdot}m^{-2}$,[11] which are close to 51.6 $mJ{\cdot}m^{-2}$ and 52.3 $mJ{\cdot}m^{-2}$ of isopropanol and acetone.[12] Thus, the ultrasonic exfoliation of TMDs is commonly performed in organic solvents with matching surface energies. However, few-layer TMDs nanosheets cannot be easily obtained using this method and the exfoliated nanosheets often exhibit a broad thickness distribution due to the strong van der Waals force between the individual layers, which leads to the poor film quality and unsatisfactory thin-film electrical performance.[13] Nevertheless, it is difficult to prepare well-dispersed few-layer TMDs

*Project supported by the National Natural Science Foundation of China (Grant Nos. 51771224, 51772087, and 51471185), the National Key R&D Program of China (Grant Nos. 2016YFJC020013 and 2018FYA0305800), and Fujian Institute of Innovation, Chinese Academy of Sciences.

†These authors contributed equally to this work.

‡Corresponding author. E-mail: htyang@iphy.ac.cn

§Corresponding author. E-mail: zhqin@hnu.edu.cn

© 2020 Chinese Physical Society and IOP Publishing Ltd

nanosheets by sonication in the most commonly used solvent, water, with a large surface energy of $\sim 100\ \mathrm{mJ\cdot m^{-2}}$.[12] Therefore, though great progress in the preparation of few or single-layer TMD nanosheets has been achieved, more facile, rapid, and versatile preparation methods for preparing high-quality aqueous-processable 2D semiconductor nanosheets are still in great demand.

In this work, we report a general approach to fast preparing highly uniform and phase-pure 2H-WSe_2 semiconducting nanosheets, which involves the pre-treatment of bulk WSe_2 crystals with supercritical carbon dioxide (SC-CO_2) exfoliation, following a mild sonication and exfoliation process in water with the assistance of a surfactant. The aqueous exfoliation of layered materials is considered as a promising technology because it allows a wide range of film-processing techniques to be applied. By precisely controlling the ionic surfactant concentration, we obtained phase-pure, few-layer 2H-WSe_2 semiconducting nanosheets with a narrow thickness and size distribution which was steadily dispersive in an aqueous solution for a long time. These WSe_2 nanosheets were then further processed into large-scale thin-film electronics by self-assembly method.

2. Experiments

All materials were purchased from Sigma-Aldrich and used without further purification. The conductivity of pure water is 18 MΩ. Bulk WSe_2 crystal powders were pretreated by SC-CO_2 exfoliation firstly. 500 g of as-received WSe_2 powders were placed in a chamber with a heater and a temperature controller. CO_2 was then liquified and added into this chamber and kept at a pressure of 10 MPa. Simultaneously, the temperature was raised to 55 °C. The WSe_2 powders were immersed in SC-CO_2 and stirred for 30 min. Then the SC-CO_2 was rapidly depressurized by opening the outlet valve.

The ultrasonic exfoliation of the pretreated WSe_2 flakes was performed by adding 20 g SC-CO_2 pretreated flakes to 400 mL of sodium deoxycholate (NaDC) aqueous solution (10 mg/mL) in a double-walled beaker. These samples were sonicated continuously for 1 h using a horn probe sonic tip (450 W, 75% amplitude, pulse rate 6 s on 2 s off). The beaker was connected to a cooling system that allowed for cold water (20 °C) to flow around the dispersion during sonification. Later, 400 mL of dispersion were centrifuged at 3000 rpm for 15 min. The sediments were discarded and the supernatant was subjected to further centrifugation of 15 min at 13000 rpm. The sediments were washed by pure water for 3 times until the residual NaDC was removed completely.

The self-assembly method was used to realize the layer-by-layer fabrication of thin film of WSe_2 nanosheets. The WSe_2 nanosheets ink was centrifugated and re-dispersed in pure water for three times to remove residual NaDC. The precipitate was dispersed in hexylamine and dropped in the hexane/ethylene glycol mixed solution. The hexylamine solution well located at the interface between hexane layer and ethylene glycol layer due to their different solubilities and densities. After complete volatilization of hexane, a SiO_2/Si or PET substrate was dipped in the ethylene glycol and the WSe_2 film was deposited on the substrate by slowly removing the ethylene glycol. The obtained WSe_2 film was treated by a mild thermal annealing (200 ℃) to remove the residual solvent and enhanced the binding strength among the nanosheets.

3. Characterization

In this work, the crystal structure of WSe_2 was analyzed through x-ray diffraction (XRD, D8 ADVANCE). Raman spectrums were collected using Raman microspectrometer (InVia Reflex, Renishaw, UK). The chemical composition of the as-prepared products was examined by x-ray photoelectron spectroscopy (XPS, R4000). The morphology of the as-prepared samples was observed using scanning electron microscope (SEM, Hitachi S-4800), and transmission electron microscope (TEM, Tecnai F20) operating at 200 kV. High angle annular dark-field (HAADF) scanning transmission electron microscope (STEM) image was obtained using JEM ARM200F TEM/STEM. The atomic force microscopy (AFM) images were obtained by using a Veeco NanoScope IV with a silicon cantilever in tapping mode. The back-gate thin-film transistors were fabricated on SiO_2/Si substrate with a 300-nm-thick oxide layer following standard photolithography and e-beam evaporation of Ti/Au (6 nm/60 nm) source/drain electrodes. The measurements of the transport characteristic were conducted at room temperature under ambient conditions by a semiconductor characterization system (Keithley 4200 SCS) with a Lakeshore probe station.

4. Results and discussion

CO_2 is commonly used as a supercritical fluid medium for its nonflammable, nontoxic nature and easily accessible critical conditions ($T_c = 31.3$ ℃, $P_c = 7.38$ MPa).[14] The WSe_2 bulk powders were treated by the supercritical CO_2 as the first step in our method. As shown in Fig. 1(a), most of the bulk WSe_2 crystals are regular hexagon with a lateral size of over 10 μm and thickness of 500 nm. However, after the supercritical treatment, the obtained WSe_2 flakes show an irregular morphology with a lateral size of about 2–5 μm and thickness of 50 nm. The edges of the WSe_2 crystals crack heavily as shown in Fig. 1(b). Since SC-CO_2 is a low surface tension fluid with high diffusivity, during the immersion and stirring of WSe_2 in SC-CO_2, CO_2 molecules with a size of 0.23 nm can easily diffuse into the interlayer space of WSe_2

with a layer distance of 0.65 nm.[14–16] After the rapid depressurization process, the intercalated CO_2 molecules widen the distance between the WSe_2 layers due to their expanded volume, which is greatly helpful to the further liquid sonication exfoliation.[15] To determine the crystalline structures, the XRD patterns were measured before and after supercritical exfoliation as shown in Fig. 1(c). After the supercritical exfoliation, all major observed diffraction peaks are consistent with those in bulk WSe_2 powders. But there is a decreasing dominant peak at around 13.8°, which is related to the (002) plane (ICDD card No. 38-1388). It indicates that bulk WSe_2 powders with high planar crystal structure are exfoliated.[17] Furthermore, the magnified XRD patterns of the (002) peaks show that the (002) peak of the SC-CO_2 pretreated WSe_2 flakes shifts to lower angle, which means that the interlayer distance is expanded because of the supercritical exfoliation.[18] Though supercritical exfoliation can be used to fabricate few-layer graphene and MoS_2 nanosheets,[16,19] few-layer WSe_2 nanosheets with a stronger van deer Waals force have to be prepared with repetitious or long-time treatments. In order to efficiently exfoliate WSe_2 nanosheets and well disperse them in water, sonication exfoliation in aqueous solution was explored to obtain few-layer WSe_2 nanosheets in a short time.

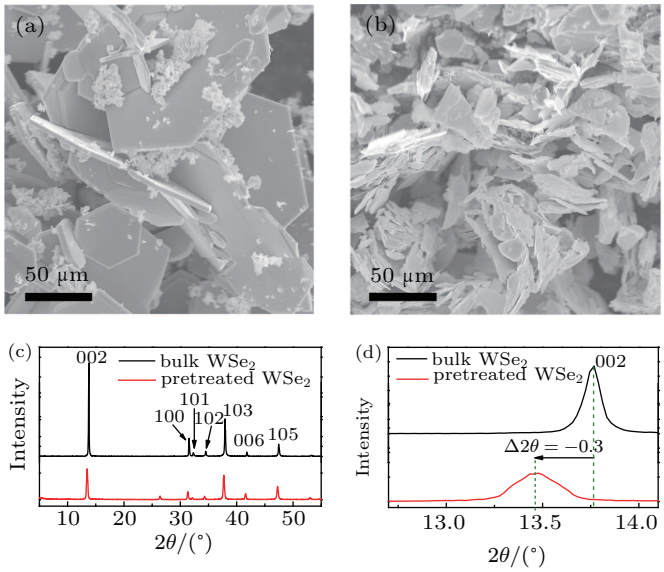


Fig. 1. SEM images of (a) original WSe_2 powders, and (b) SC-CO_2 pre-treated WSe_2 powders. (c) XRD patterns of original and SC-CO_2 pretreated WSe_2 powders. (d) Magnified XRD patterns of the (002) peaks in (c).

Sonication waves generate unstable cavitation bubbles that collapse into high-energy jets, which are large enough to break up layered crystals and produce exfoliated nanosheets.[20] The key problem is to prevent rapid reaggregation of the nanosheets due to the mismatch of the surface energy between TMDs and water. To solve this problem, NaDC, a kind of anionic detergent, was selected to decrease the surface energy of water and stabilize the nanosheets as an ionic surfactant. The NaDC molecular chain is about 1.5 nm long resulting in an enough distance to decrease the binding force between the nanosheets since the interlayer spacings of most TMDs are about 0.7 nm. The equilibrium contact angles of different solvents on the WSe_2 substrate can decrease from 49.2° of pure water to 26.3° of NaDC aqueous solution, and to 11.2° of 50% ethanol aqueous solution, which indicates that the surface energy of water can effectively regulate by NaDC and ethanol. As a comparation, N-methyl pyrrolidone (NMP) with the contact angle of 6.1° was also used to sonicate WSe_2 powder. The pretreated WSe_2 powders were sonicated for 1 h in NaDC aqueous solution, pure water, 50% ethanol aqueous solution, and NMP, respectively. Among them, the best quality of the as-prepared WSe_2 nanosheets is obtained in the NaDC aqueous solution, a better case is in 50% ethanol aqueous solution, and the worst case is in water or NMP. These results confirm that a solvent with a match surface energy is of benefit to the liquid exfoliation of TMDs. As shown in Fig. 2(a), the resultant WSe_2 nanosheets can well disperse in NaDC aqueous solution with a concentration of 5 mg/mL and stay stable as a uniform colloidal suspension for more than six months. The concentration of the WSe_2 nanosheets could be tuned from 0.1 mg/mL to 10 mg/mL by centrifugation and redispersion in proper solvents for specific applications. The typical TEM image of few-layered WSe_2 nanosheets prepared in the NaDC aqueous solution is shown in Fig. 2(b). The well-dispersed WSe_2 nanosheets have an average size of 59.7 nm determined over 200 nanosheets by the major axis and a size distribution of less than 10%. The samples sonicated in other solvents show thick nanosheets or a poor dispersivity. Atomic force microscopy was used for assessing the thicknesses of these 2D WSe_2 layers and a clear height profile across the nanosheet of 5.0 nm was observed, corresponding to 5–7 layers of WSe_2 nanosheets as shown in Fig. 2(c). It should be noted that if the supercritical exfoliation is absent, WSe_2 nanosheets are too large and thick after direct sonication exfoliation even under a stronger sonication exfoliation treatment. It indicates that supercritical exfoliation as the pretreatment step, is vital for the production of few-layer WSe_2 nanosheets with high-quality. High-resolution scanning TEM (STEM) was performed on an aberration corrected scanning transmission electron microscope for investigating the structure of the WSe_2 nanosheets. Owing to the different atomic arrangements of 2H and 1T structures, their direct identification is possible with HAADF STEM imaging. Figure 2(d) shows the HAADF STEM image of the WSe_2 nanosheets. The lattice spacing of 0.28 nm corresponds to the (100) plane of 2H-WSe_2, which agrees with the results from the fast Fourier transform (FFT) pattern. In Fig. 2(e), the signal intensity of atoms along the red line shows the same value since the signals from the Se sites in the top layer overlap with those from the W sites in the bottom layer

in 2H-WSe_2 along the electron beam direction. Moreover, the crystalline structures are still intact after the sonication exfoliation, which indicates that the molecular-assisted sonication can exfoliate the WSe_2 powder at low sonication power. It should be noted that the mild sonication exfoliation method in the NaDC aqueous solution can also be applied for the preparation of other 2D crystals nanosheets.

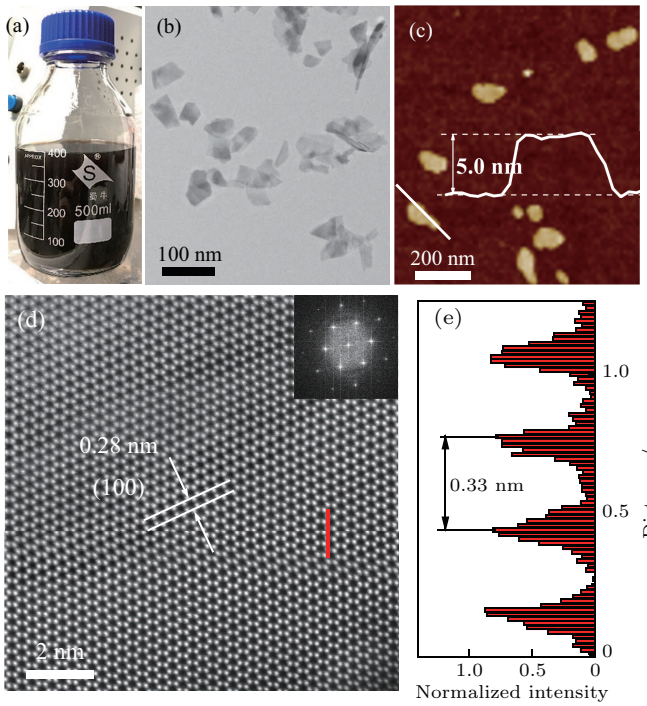


Fig. 2. (a) Photograph of exfoliated WSe_2 nanosheets dispersed in aqueous NaDC solution. (b) TEM and (c) AFM images of WSe_2 nanosheets, the inset pattern in (c) is the cross-sectional height profile. (d) HAADF STEM image of WSe_2 nanosheets, the FFT pattern is shown in the inset. (e) The signal intensity of atoms along the red line in (d) showing the same contrast value, corresponding to the lattice constant of 0.33 nm.

The as-prepared WSe_2 nanosheets were further washed over three times to remove any impurities. The Raman spectrum of the WSe_2 nanosheets is shown in Fig. 3(a). Three characteristic peaks at 135 cm^{-1}, 249 cm^{-1}, and 308 cm^{-1} are assigned to E_{1g}, E^1_{2g}, and B^1_{2g} modes, which are in good agreement with those of mechanically exfoliated few-layer samples, suggesting the absence of significant strain and defect in our samples.[21] Additionally, the chemical composition of the exfoliated WSe_2 was examined by XPS. In Fig. 3(b), two obvious peaks at 34.28 eV and 32.08 eV are attributed to W $4f_{5/2}$ and W $4f_{7/2}$, respectively. The small peak at 38.1 eV is attributed to W $5p_{3/2}$. The peaks at 54.18 eV and 54.38 eV in Fig. 3(c) correspond to Se $3d_{5/2}$ and Se $3d_{3/2}$, respectively, confirming the formation of Se^{2-}, which agrees with the spectrum of pristine 2H-WSe_2.[21] The lack of any Na signal in XPS spectrum can be proved by Fig. S6. These results indicate that the WSe_2 nanosheets are neither oxidized nor covalently functionalized with impurity species such as NaDC after the supercritical exfoliation and sonication exfoliation.

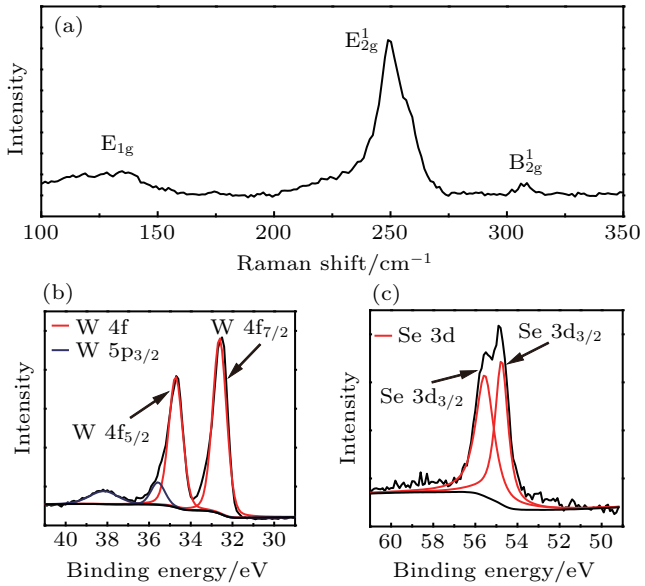


Fig. 3. (a) Raman spectrum of WSe_2 nanosheets. XPS spectra of (b) W 4f and (c) Se 3d.

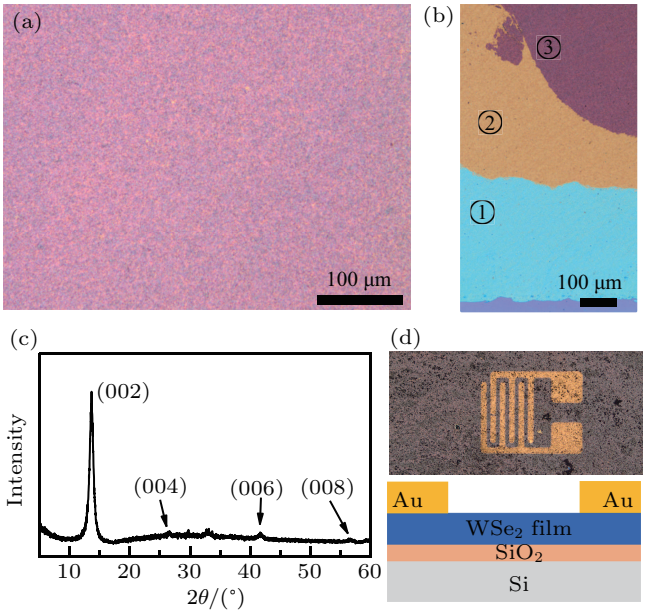


Fig. 4. (a) Optical image of a smooth thin film of WSe_2 nanosheets. (b) Optical image of layer-by-layer self-assembly thin film of WSe_2 nanosheets. Numbers 1–3 indicate the layers of WSe_2 films, the regions with different colors show the films with different thicknesses. (c) XRD pattern of the resulting thin film displaying only {001} planes. (d) Schematic configuration and optical images of the back-gate WSe_2 thin-film transistors on the 300-nm-thick SiO_2/Si substrate.

Based on the stable WSe_2 nanosheet ink, large-area thin films can be prepared on diverse substrates using various solution-processing approaches such as spin-coating, self-assembly, and dipping coating. Alternatively, the ink solution may be applied to produce thin films of larger area by using the industrial roll-to-roll coating process. Herein, considering the well-dispersed state of the WSe_2 nanosheets with a size of dozens of nanometers, we tried to obtain a more smooth film by using a self-assembly technique at two-phase interface.[22–24] We realized the high-quality 2D semiconducting thin films with a large area of 10 mm×10 mm by the layer-

by-layer self-assembly technique as shown in Fig. 4(a). Figure 4(b) shows the boundaries of the different self-assembly layers with the thicknesses of 100 nm, 150 nm, and 200 nm for the first, second, and third layers, respectively. The XRD pattern of the resulted thin film exhibits only {001} planes (Fig. 4(c)), indicating the well-controlled assembly of the WSe_2 nanosheets along the *c* axis of the crystal and the broad-area plane-to-plane contacts between the nanosheets. The high-quality WSe_2 semiconducting thin films with different self-assembly layers can be further processed using standard photolithography to create desired patterns for the fabrication of arrays of devices. It should be noted that a continuous film is difficult to form using a spin-coating process with our WSe_2 nanosheets. To explore the potential of the thin films for device applications, we fabricated back-gate transistors on 300-nm-thick SiO_2/Si substrate based on the self-assembled WSe_2 thin films. The Ti (5 nm)/Au (60 nm) electrodes were defined directly on the WSe_2 thin films through a shadow mask by thermal evaporation (as shown in Fig. 4(d)). The channel width (W) and equivalent channel length (L) of the device are 20 μm and 2000 μm, respectively.

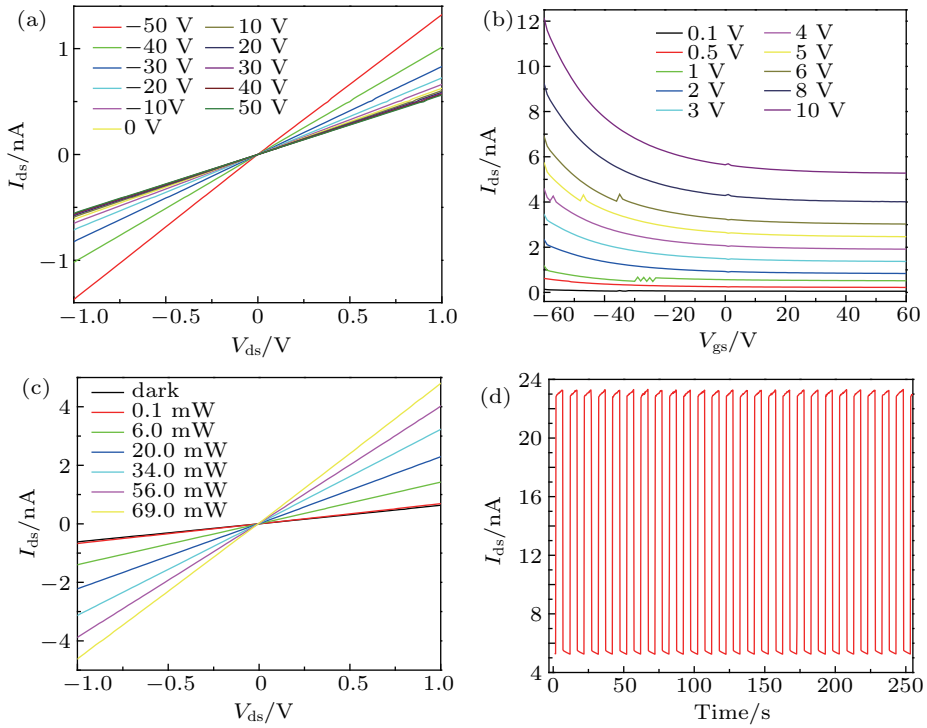


Fig. 5. (a) Typical output characteristics and (b) transfer characteristics of the WSe_2 transistors. (c) Photocurrent under different laser powers and (d) transient photoresponsivity characteristics of the WSe_2 transistors. All measurements were carried out with 650 nm wavelength under a zero gate–source bias.

Typical output curve and transfer curves of the field-effect transistors are shown in Figs. 5(a) and 5(b), respectively, where V_{gs} is the gate voltage, I_{ds} is the source–drain current, and V_{ds} is the source–drain bias. The linear output curves in Fig. 5(a) demonstrate the formation of ohmic contacts in the WSe_2/Au electrodes. The WSe_2 transistor exhibits a p-type transport behavior with an on/off ratio of ~ 2.8 and an on-state current of ~ 12 nA at $V_{ds} = 10$ V. The weak gate tunability may be due to the large thickness of the WSe_2 film. The field-effect electron mobility in the transistor was extracted from the linear regime of the transfer curve using the standard formula $\mu = \frac{dI_{sd}}{dV_g} \cdot \frac{L}{W} \cdot \frac{1}{C_g V_{sd}}$, where W is the width of the channel, L is the length of the channel, C_g is the capacitance per unit area of the gate dielectric, V_{ds} is the applied source–drain bias, and dI_{ds}/dV_g is the slope of the linear part of the transfer plot. From the transfer characteristics, the extracted field effect carrier mobility is about 0.12 $cm^2 \cdot V^{-1} \cdot s^{-1}$. The carrier mobility in our large-area WSe_2 thin films obtained by the facile solution-processed method is higher than that reported in previous solution processed and MOCVD fabricated WSe_2 thin films (~ 0.08 $cm^2 \cdot V^{-1} \cdot s^{-1}$).[25,26] While it is smaller than that reported in few-layer WSe_2 nanosheets obtained by chemical vapor deposition (CVD; 7.3 $cm^2 \cdot V^{-1} \cdot s^{-1}$).[27] Though the performance of our solution-processed device could be improved by further optimization, the present results indicate that the contacts between WSe_2 nanosheets in the large-area thin film do not greatly hinder the transport properties of the thin film, owing to the charge transport across the stacked nanosheets due to the broad-area dangling-bond-free plane-to-plane contacts between them. Such contacts are advantageous compared with the point-to-point contacts in zero-dimensional quantum-dot thin films and in one-dimensional nanowire thin films, which, as mentioned previously, have considerable interfacial dangling bonds and chemical disorder. With a sta-

ble ink solution and a relatively low processing temperature, thin-film devices can also readily be prepared on flexible plastic substrates with comparable electronic performance such as polyethylene terephthalate (PET) and polyimide (PI), which demonstrates the potential of the 2D semiconductor ink for flexible and wearable electronics.

Since WSe_2 has a direct bandgap of 1.6 eV in monolayer and an indirect bandgap of 1.2 eV in bulk, it has not only been widely used for field-effect transistors (FETs) but also for optoelectronic applications owing to its tunable energy bands, strong optical absorption, and ultrafast charge transfer. We extracted the photocurrent and photoresponsivity of the WSe_2 thin film transistor and analyzed its transient response as shown in Figs. 5(c) and 5(d). The photocurrent at room temperature is defined as the difference between the currents measured in dark state and under light illumination, i.e., $I_{ph} = I_{illumination} - I_{dark}$. Figure 5(c) presents the drain to source current I_{ds} as a function of the source–drain bias V_{ds} under different illumination powers from 0 (dark state) to 69 mW of a $\lambda = 650$ nm laser source. These data were collected in absence of gate voltage ($V_{gs} = 0$ V). The I_{ds} displays a linear dependence on V_{ds} under different illumination powers, which is primarily attributed to the significant reduction of Schottky barriers allowing the photo-generated carriers to transport efficiently through the WSe_2/metal interface. The photocurrent can arrive at 4 nA at $V_{ds} = 1$ V and increases with the light power, which demonstrates that the electron–hole pair generation is almost proportional to the absorbed photon flux.[28] The photoresponsivity R is the ratio between I_{ph} and the applied illumination power P. The time-resolved photoresponse of the WSe_2 thin film is displayed in Fig. 5(d). The maximum responsivity reaches 0.26 μA/W at $V_{ds} = 5$ V and 0.05 μA/W at $V_{ds} = 1$ V. The response time and the recovery time are 0.2 s and 0.3 s at $V_{ds} = 5$ V according to the rising and falling edges, respectively. While, the response time and the recovery time are 0.3 s and 0.3 s at $V_{ds} = 1$ V. Thus, the WSe_2 thin film is demonstrated to display significant potential for future optoelectronic applications.

5. Conclusion

We demonstrate a rapid and scalable method to prepare WSe_2 nanosheets. After treatment with SC-CO_2, WSe_2 flakes are partially exfoliated with enlarged layer distance. Subsequently, the SC-CO_2 pretreated WSe_2 flakes are exfoliated into few-layer nanosheets by ultrasonication in water, resulting in a well dispersive colloid solution without any precipitate even after half a year. The crystal structures and physical properties are still intact after the exfoliation process. Good dispersivity and uniformity enable these nanosheets to self-assembly into thickness-controlled thin films for scalable fabrication of large-area arrays of thin-film transistors. Furthermore, our SC-CO_2 treatment and sonication exfoliation strategy can generally be applied to a wide range of layered 2D materials, to establish a library of 2D-material inks with diverse properties. Our study thus provides a robust pathway to scalable production of high-quality nanosheets for large-area electronics and optoelectronics.

References

[1] Wang Y, Kim J C, Wu R J, Martinez J, Song X, Yang J, Zhao F, Mkhoyan A, Jeong H Y and Chhowalla M 2019 *Nature* **568** 70
[2] Lien D H, Uddin S Z, Yeh M, Amani M, Kim H, Ager III J W, Yablonovitch E and Javey A 2019 *Science* **364** 468
[3] Meng X, Yu L, Ma C, Nan B, Si R, Tu Y, Deng J, Deng D and Bao X 2019 *Nano Energy* **61** 611
[4] Smith R J, King P J, Lotya M, Wirtz C, Khan U, De S, O'Neill A, Duesberg G S, Grunlan J C, Moriarty G, Chen J, Wang J Z, Minett A I, Nicolosi V and Coleman J N 2011 *Adv. Mater.* **23** 3944
[5] Omelianovych A Y, Dominskiy D I, Feldman E V, Bessonov A A, Stevenson K J and Paraschuk D Y 2017 *J. Mater. Sci.: Mater. Electron.* **28** 18106
[6] Li L, Guo Y, Sun Y, Yang L, Qiu L, Guan S, Wang J, Qiu X, Li H, Shang Y and Fang Y 2018 *Adv. Mater.* **30** 1706215
[7] Yan B, Zhang B, Nie H, Li G, Sun X, Wang Y, Liu J, Shi B, Liu S and He J 2018 *Nanoscale* **10** 20171
[8] Yin J, Zhu F, Lai J, Chen H, Zhang M, Zhang J, Wang J, He T, Zhang B, Yuan J, Yan P and Ruan S 2019 *Adv. Opt. Mater.* **7** 1801303
[9] Xia J, Chao D, Chen Z, Liu Z, Kuo J, Yan J and Shen Z X 2017 *Nanoscale* **9** 7533
[10] Kim T, Kim J, Park I, Cho K and Choi S 2019 *2D Mater.* **6** 025025
[11] Shen J, He Y, Wu J, Gao C, Keyshar K, Zhang X, Yang Y, Ye M, Vajtai R, Lou J and Ajayan P M 2015 *Nano Lett.* **15** 5449
[12] Shen J, Wu J, Dong M, Xu P, Li J, Zhang X, X, Yuan J, Wang X, Ye M, Vajtai R, Lou J and Ajayan P M 2016 *Small* **12** 2741
[13] Lin Z, Liu Y, Halim U, Ding M, Liu Y, Wang Y, Jia C, Chen P, Duan X, Wang C, Song F, Li M, Wan C, Huang Y and Duan X 2018 *Nature* **562** 254
[14] Pu N W, Wang C A, Sung Y, Liu Y M and Ger M D 2009 *Mater. Lett.* **63** 1987
[15] Wang Y, Chen Z, Wu Z, Li Y, Yang W and Li Y 2018 *Langmuir* **34** 7797
[16] Rizvi R, Nguyen E P, Kowal M D, Mak W H, Rasel S, Islam M A, Abdelaal A, Joshi A S, Zekriardehani S, Coleman M R and Kaner R B 2018 *Adv. Mater.* **30** 1800200
[17] Qi Y, Xu Q, Wang Y, Yan B, Ren Y and Chen Z 2016 *ACS Nano* **10** 2903
[18] Zheng J, Zhang H, Dong S, Liu Y, Nai C T, Shin H S, Jeong H Y, Liu B and Loh K P 2014 *Nat. Commun.* **5** 2995
[19] Tian X, Wu J, Li Q, Li Y, Chen Z, Tang Y and Li Y 2018 *J. Mater. Sci.* **53** 7258
[20] Qiao W, Yan S M, He X M, Song X Y, Li Z W, Zhang X, Zhong W and Du Y W 2014 *RSC Adv.* **4** 50981
[21] Li H, Lu G, Wang Y, Yun Z, Cong C, He Q, Wang L, Ding F, Yu T and Zhang H 2013 *Small* **9** 1974
[22] Yu X, Prévot M S, Guijarro N and Sivula K 2015 *Nat. Commun.* **6** 7596
[23] Lei W J, Xu J J, Yu Y S, Yang W W, Hou Y L and Chen D F 2018 *Nano Lett.* **18** 7839
[24] Yang W W, Yu Y S, Wang L, Yang C H and Li H B 2015 *Nanoscale* **7** 2877
[25] Kelly A G et al All-printed thin-film transistors from networks of liquid-exfoliated nanosheets. 2017 *Science* **356** 69
[26] Gong Y Y, Zhang X T, Redwing J M and Jackson T N 2016 *J. Elec. Mater.* **45** 6280
[27] Zhang W J, Chiu M H, Chen C H, Chen W, Li L J and Wee A T 2014 *ACS Nano* **8** 8653
[28] Cheng F, He B 2016 *Chin. Phys. Lett.* **33** 57301